Monthly Notices
of the
ROYAL ASTRONOMICAL SOCIETY

Mon. Not. R. Astron. Soc. **417,** 1140–1147 (2011) doi:10.1111/j.1365-2966.2011.19335.x

Studying the long-time variability of the Seyfert 2 galaxy NGC 4388 with *INTEGRAL* and *Swift*

E. V. Fedorova,[1⋆] V. Beckmann,[2] A. Neronov[3,4] and S. Soldi[5]

[1]*Astronomical Observatory of the Kiev Tarass Schevchenko University, Kiev 03040, Ukraine*
[2]*François Arago Centre, APC, Université Paris Diderot, CNRS/IN2P3, CEA/DSM, Obs. Paris, 13 rue Watt, 75205 Paris Cedex 13, France*
[3]*ISDC Data Centre for Astrophysics, Chemin d'Écogia 16, 1290 Versoix, Switzerland*
[4]*Observatoire Astronomique de l'Université de Genève, Ch. Des Maillettes 51, 1290 Sauverny, Switzerland*
[5]*Laboratoire AIM - CNRS - CEA/DSM - Université Paris Diderot (UMR 7158), CEA Saclay, DSM/IRFU/SAp, 91191 Gif-sur-Yvette, France*

Accepted 2011 June 27. Received 2011 June 24; in original form 2010 July 29

ABSTRACT

We present analysis results on the Seyfert 2 galaxy NGC 4388 based on 6 yr of *INTEGRAL* data combined with *Swift*/Burst Alert Telescope survey and *Swift*/X-Ray Telescope pointed observations. These data, taken from 2003 to 2009, allow us to study the broad-band properties of this active galactic nucleus in the 0.3–300 keV energy range. The continuum emission of NGC 4388 is well represented by an absorbed power-law model with exponential cut-off at high energies and an upper limit on the reflection component of $R < 0.5$. We find slow strong variations of the hard X-ray emission, indicating both flux and spectral slope changes on the 3–6 months time-scale. In comparison with previous results on NGC 4388, the source shows a complex variability behaviour, i.e. the spectral shape and the 20–60 keV flux vary independently.

Key words: X-rays: galaxies – galaxies: nuclei – galaxies: Seyfert.

1 INTRODUCTION

The unification model of active galactic nuclei (AGN) assumes that the main difference between the various AGN types is due to geometrical effects (e.g. Antonucci 1993). The emission around the supermassive black hole at the AGN core is thought to be absorbed by more or less matter, causing the different characteristics we see in type 1 and type 2 objects. These differences should disappear when studying Seyfert galaxies at hardest X-rays (i.e. $E \gg 10$ keV) where the role of absorption can be neglected, unless the absorbing material is indeed Compton thick. The hard X-ray emission can be studied in view of its spectral shape as well as for spectral variations in time. Only in recent years, with the hard X-ray detectors on-board *BeppoSAX*, *International Gamma-ray Astrophysical Laboratory* (*INTEGRAL*) and *Swift*, these kind of studies became feasible.

NGC 4388 is the brightest Seyfert 2 galaxy in hard X-rays (Beckmann et al. 2004), with a redshift $z = 0.0084$ and viewed nearly edge-on at an inclination angle $i \simeq 72^\circ$ (Phillips & Malin 1982). The mass of the black hole in the centre of this AGN is estimated to be $M_{\rm BH} = (1.7 \pm 0.4) \times 10^7\,{\rm M}_\odot$ (Bian & Gu 2007). Its X-ray emission is absorbed by a moderate (by the scales of Seyfert 2 galaxies) and variable hydrogen column density in the range $10^{23} < N_{\rm H} < 10^{24}\,{\rm cm}^{-2}$ (Hanson et al. 1990; Elvis et al. 2004), and thus can be classified as 'Compton-thin Seyfert 2' galaxy following Dewangan (2001).

Because of its brightness, NGC 4388 has been observed by all major X-ray and γ-ray missions. The earliest X-ray observation of this object was done by Spacelab 2-X-Ray Telescope (SL2-XRT), detecting a column density of the absorbing medium at a level of $N_{\rm H} \simeq 10^{23}\,{\rm cm}^{-2}$ (Hanson et al. 1990). Later the source has been observed by *ROSAT* and *ASCA*, and an Fe Kα emission line near 6.4 keV and a thermal component in the soft X-rays were found (Iwasawa et al. 1997; Forster, Leighly & Kay 1999). The complex structure of the circumnuclear region with the X-ray bright nebula surrounding the central part was investigated in using the *Chandra* observations of NGC 4388 (Iwasawa et al. 2003). Finally, the results of both *XMM–Newton* and *RXTE* observations had shown that the density of the absorbing medium is strongly variable (Elvis et al. 2004).

The first broad-band view on this source has been performed by *BeppoSAX*, disclosing the first signs of a Compton reflection and a high-energy cut-off above 100 keV in its spectrum (Risaliti 2002). The source was also detected in the course of the *Swift*/Burst Alert Telescope (BAT) All-Sky Survey, appearing to be variable in the energy range 14–195 keV (Beckmann et al. 2007a; Tueller et al. 2008). Observations by *Suzaku* (Fukazawa et al. 2007a; Shirai et al. 2008) suggest the presence of both direct and reflected components in the spectrum and detected fast (hour-scale) variations

⋆E-mail: efedorova@ukr.net

of the direct nuclear component of NGC 4388's X-ray to γ-ray emission.

NGC 4388 exhibits properties of both type 1 and type 2 AGN. The X-rays show a high level of absorption, clearly above the common dividing line at $N_{\rm H} = 10^{22}$ cm^{-2}, and a Compton reflection component (Fukazawa et al. 2007a; Shirai et al. 2008), indicating that the source belongs to the type 2 class. On the other hand in the second SL2-XRT observation of NGC 4388 a low level of hydrogen column density had been detected (Elvis et al. 2004). NGC 4388 and other type 2 AGN have been shown to host a hidden broad line region (HBLR), visible in polarized light (Bian & Gu 2007). Studying the Eddington ratio $\lambda = L_{\rm bol}/L_{\rm Edd}$ (here $L_{\rm bol}$ is the bolometric luminosity and $L_{\rm Edd}$ the Eddington luminosity) for HBLR ($\lambda = 0.85 \pm 0.31$) and non-HBLR ($\lambda = 0.33 \pm 0.12$) Seyfert 2 galaxies, Bian & Gu (2007) find that NGC 4388 displays a strong accretion flow with $\lambda = 0.79$, typical for a Seyfert 2 with a HBLR.

Since its first detection by *INTEGRAL* (Winkler et al. 2003) in 2002 (Courvoisier et al. 2003b), NGC 4388 has been observed several times over the years. The *INTEGRAL* mission offers the unique possibility to perform simultaneous observations over the 3–8000 keV energy range. This is achieved by the X-ray monitor [Joint European X-Ray Monitor (JEM-X)] (3–35 keV; Lund et al. 2003), the soft gamma-ray imager [Imager on Board *INTEGRAL* Spacecraft (IBIS)/*INTEGRAL* Soft Gamma-Ray Imager (ISGRI)] (20–1000 keV; Lebrun et al. 2003) and the spectrograph Spectrometer aboard *INTEGRAL* (SPI; Vedrenne et al. 2003), which operates in the 20–8000 keV region. Each of these instruments employs the coded-aperture technique (Caroli et al. 1987). In addition to these instruments an optical monitor (OMC; Mas-Hesse et al. 2003) provides photometric measurements in the *V* band. The first detailed analysis of IBIS/ISGRI and SPI data of NGC 4388 from the first year of observations was presented in Beckmann et al. (2004). The NASA-led *Swift* mission (Gehrels et al. 2004), launched in 2004, provides a more homogeneous sky coverage in the 15–195 keV band through the BAT instrument (Barthelmy et al. 2005) because of its observation strategy following gamma-ray bursts, making it an ideal instrument for long-term hard X-ray variability studies. The *INTEGRAL*'s hard X-ray imager IBIS/ISGRI is more sensitive though and extends up to several hundred keV with better spectral resolution.

In this paper we present the results of our study of the X-ray and γ-ray emission of NGC 4388 detected by *INTEGRAL* based on 6 yr of observations. Our goal is to investigate the 3–300 keV continuum emission, using a larger data set than considered in previous works (Beckmann et al. 2004, 2009). The longer accumulated exposure time enables us to achieve better statistics and to detect the high-energy cut-off or/and the reflection component in the hard X-ray domain. In addition, we investigate the long-term variability properties of the source.

The outline of the paper is as follows. In Section 2 we describe the data set and the analysis methods. Section 3 is devoted to the results of the spectral analysis based on the full *INTEGRAL* data set. Combining the spectra from different instruments on-board *INTEGRAL* we obtain the spectrum of the source in the 3–300 keV energy range and detect the high-energy cut-off in the spectrum. In Section 4 we study the variability of the AGN and find significant variations of the ISGRI 20–60 keV flux as well as in the 15–50 keV data provided by *Swift*/BAT. The spectral shape is found to vary and the changes are not directly related to the flux level of the source. Finally, in Section 5 we discuss our results and compare them with the results of other X-ray and γ-ray observations.

Table 1. *INTEGRAL* observation log for NGC 4388.

Data rev	Start date (UTC)	ISGRI exp. (ks)	SPI exp. (ks)	JEM-X exp. (ks)
028	2003-01-05T12:05	116.5	14.9	0
030	2003-01-11T07:50	10.2	0	0
032	2003-01-17T09:44	98.8	20.7	0
036	2003-01-30T04:18	42.5	0	0
071	2003-05-14T07:44	23.0	0	0
072	2003-05-17T01:10	38.1	0	0
078	2003-06-04T14:58	3.1	0	0
082	2003-06-16T06:48	34.6	0	0
089	2003-07-07T09:32	77.6	0	0
090	2003-07-09T20:32	47.8	0	0
093	2003-07-18T17:03	20.5	0	0
094	2003-07-21T16:44	122.8	0	126.2[a]
148	2004-01-01T17:00	12.8	0	0
149	2004-01-02T06:41	7.8	0	0
207	2004-06-23T18:35	71.6	12.6	0
267	2004-12-20T19:41	87.1	11.9	0
268	2004-12-23T15:51	85.9	14.0	0
270	2004-12-29T05:17	86.9	14.0	0
272	2005-01-04T10:07	67.2	12.0	0
273	2005-01-07T04:08	86.2	15.3	0
274	2005-01-11T10:07	35.4	0	0
275	2005-01-18T04:54	34.3	0	0
317	2005-05-19T06:32	39.3	0	0
318	2005-05-21T18:20	33.2	0	0
320	2005-05-28T05:45	127.7	73.0	16.4
321	2005-05-30T17:44	84.1	66.0	10.4
324	2005-06-09T02:20	38.6	0	0
325	2005-06-11T23:16	6.8	0	0
334	2005-07-09T10:13	103.7	39.3	8.2
397	2006-01-13T20:06	10.2	0	0
398	2006-01-17T04:31	10.2	0	0
399	2006-01-20T01:29	3.4	0	0
443	2006-05-30T11:20	102.9	56.6	18.6
444	2006-06-02T20:27	100.7	55.8	6.1
445	2006-06-05T23:45	99.9	61.4	22.0
633	2007-12-19T17:54	152.9	40.0	0
635	2007-12-25T17:38	169.9	41.0	0
637	2007-12-31T17:12	166.2	37.2	0
747	2008-11-25T19:14	110.4	121.2	30.0
748	2008-11-28T18:21	130.4	132.1	41.3
749	2008-12-01T18:15	107.3	133.4	18.7
750	2008-12-04T21:01	102.6	91.0	24.2
751	2008-12-08T01:29	103.4	109.8	33.0
752	2008-12-11T03:52	88.0	97.5	24.3
753	2008-12-13T23:26	107.4	113.6	20.4
754	2008-12-17T19:07	40.7	0	37.5
758	2008-12-28T04:31	180.0	114.8	40.8
759	2008-12-30T16:05	56.0	25.1	17.2
762	2009-01-10T02:53	7.6	0	0
Total	01/2003–01/2009	4252.2	1524.1	493.3

[a]This is the only revolution with JEM-X2 data for NGC 4388.

2 DATA ANALYSIS

A summary of the *INTEGRAL* observations that are analysed in this paper is given in Table 1. The data sample includes all publicly available *INTEGRAL* data on the source as of 2009 June, i.e. 1344 science windows (ScWs)[1] from spacecraft revolutions up to 762

[1] A ScW is an *INTEGRAL* data set based on typically 2 ks of observation.

Table 2. *Swift*/XRT observation log for NGC 4388.

Data set	Observation date	XRT exp. time (ks)	Flux (cts)	Counts
00035464001	2005-12-27T02:02	13.5	1.89 ± 0.18	821
00035464002	2006-07-08T11:06	9.0	3.62 ± 0.3	1278
00035464003	2006-07-27T00:06	7.8	2.57 ± 0.22	910
00037262001	2008-05-09T04:35	1.7	0.35 ± 0.04	125
Total	–	32.0	2.1 ± 0.2	3134

for the IBIS/ISGRI instrument. For SPI and both JEM-X monitors there were 586 and 154 ScWs, respectively. The total exposure time of the data set used for the light-curve extraction is ∼4.2 Ms for the imager IBIS/ISGRI, including all observations in which NGC 4388 was at less than 15° off-axis angle. To extract the spectra we have used a smaller data set (from the area within the 10° off-axis angle) of 840 ScWs (total exposure ∼2.1 Ms). For the spectrometer SPI ∼1.5 Ms of data are available (off-axis angle <10°), and the two X-ray monitors accumulated a total exposure time of ∼500 ks (off-axis angle <3°) on the source.

INTEGRAL IBIS/ISGRI data analysis was performed using version 7.0 of the Offline Scientific Analysis (OSA) software provided by the *INTEGRAL* Science Data Centre (ISDC; Courvoisier et al. 2003a). For IBIS/ISGRI spectral extraction the standard software was used. Spectra were extracted for every individual ScW and then summed up for the whole data set. The source is detected up to 300 keV. In order to account for (inter)calibration uncertainties, we applied 3 per cent systematics to the *INTEGRAL* spectra. The significances of detection are 105σ (20–40 keV), 60σ (40–60 keV), 37σ (60–100 keV) and 8σ (100–200 keV). For the JEM-X data we used OSA 9, and we extracted the spectra from mosaic images in several energy bands. This procedure has been shown to be more reliable for sources below ∼20 mCrab than the standard spectral extraction. The data from JEM-X1 and JEM-X2 have been merged, which gives a total exposure time of 493 ks and a detection significance of 45σ in the 3–35 keV energy band. SPI analysis was performed using the SPIROS (version 9.3.2) software, which is identical in OSA 8 and OSA 9.

The IBIS/ISGRI light curves have been extracted in three energy bands (20–60, 60–100 and 100–200 keV). The light curves are based on individual ScW and have been rebinned into 1 to 5 d bins, depending on the exposure time of the particular *INTEGRAL* revolution.

The *Swift*/BAT light curve in the 15–50 keV energy band for the years 2005–2009 has been obtained from the 'Scaled Map Transient Analysis' of NGC 4388 provided by the *Swift*/BAT team.[2]

All the four pointed observations of NGC 4388 by *Swift*/XRT have been performed in photon counting mode. We merged all the four *Swift*/XRT spectra into one using the standard XSELECT routine and the XRT pipeline version 0.12.4 (HEASOFT 6.8 package). The source counts for this spectrum were collected from a 25 arcsec circular area around the source and the background was determined from a circular off-source region of equal size. The observation logs for the XRT data of NGC 4388 are shown in Table 2.

[2] http://heasarc.gsfc.nasa.gov/docs/swift/results/transients/

3 SPECTRAL MODELLING

Spectral modelling of the data was done using the XSPEC 12 package of HEASOFT 6.9 (Arnaud 1996). For the spectral analysis we considered the two following models which describe the effect of reflection of the primary AGN emission on either the accretion disc, a hot corona or the cold absorbing gas surrounding it (see e.g. Risaliti 2002 for a physical motivation of the choice of the spectral models):

(i) an absorbed power-law model with cold Compton reflection component (XSPEC model zwabs·reflect(po); Magdziarz & Zdziarski 1995). The reflection strength R is defined as the relative amount of reflection compared to the directly viewed primary spectrum;

(ii) an absorbed power-law model with additional cold Compton reflection component and exponential cut-off at high energies (zwabs·pexrav model; Magdziarz & Zdziarski 1995).

The combined *Swift*/XRT and corresponding quasi-simultaneous ISGRI spectrum (i.e. obtained from revolutions 334 to 637, see Tables 1 and 2) are shown in Fig. 1. The best-fitting results are shown in Table 3, where the *Swift*/XRT and quasi-simultaneous IBIS/ISGRI spectra are denoted as data set 1. The data set 2 includes all the *INTEGRAL* data, i.e. JEM-X, IBIS/ISGRI and SPI, obtained during the whole time of observations.

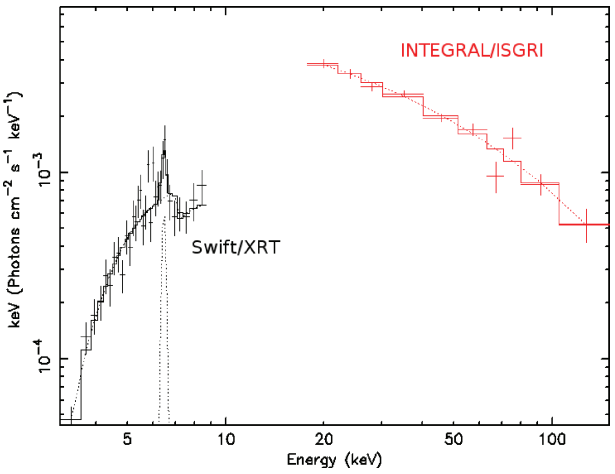

Figure 1. Unfolded *Swift*/XRT spectra with quasi-simultaneous *INTEGRAL* IBIS/ISGRI spectrum.

Table 3. The best-fitting model (ii) parameters to the averaged *INTEGRAL* and *Swift*/XRT spectra with the errors at 90 per cent confidence level.

Parameter	Data set 1[a]	Data set 2[b]
χ^2/dof	40.0/34	19.4/18
Γ	1.34 ± 0.02	1.70 ± 0.04
E_C (keV)	75^{+7}_{-6}	209^{+44}_{-32}
R	<0.5	<0.5
N_H (10^{23} cm^{-2})	3.0 ± 0.2	$4.0^{+1.2}_{-1.0}$
$F_{4-20\,keV}$ [c]	1.35 ± 0.11	1.52 ± 0.09
$F_{20-60\,keV}$ [c]	1.54 ± 0.03	1.41 ± 0.02
$F_{60-200\,keV}$ [c]	1.34 ± 0.30	1.56 ± 0.02
K_X	$0.69^{+0.18}_{-0.04}$	1.02 ± 0.13
K_γ	–	0.71 ± 0.15

[a] XRT+quasi-simultaneous ISGRI spectra.
[b] ISGRI+JEM-X+SPI spectra.
[c] Unabsorbed flux in units of 10^{-10} erg cm^{-2} s^{-1}.

In order to account for the different observational periods and for uncertainties in the cross-calibration, we applied intercalibration factors K_X and K_γ for the X-ray spectrum (obtained by JEM-X or XRT) and the SPI spectrum, respectively, with respect to the ISGRI spectrum. The unabsorbed fluxes in three energy bands (4–20, 20–60 and 60–200 keV) are given in Table 3.

We did not include the Fe Kα line seen e.g. in *XMM–Newton* data (Elvis et al. 2004; Beckmann et al. 2004) when fitting the data set 2 because the spectral resolution and effective exposure time of the JEM-X instruments did not allow a significant detection.

When analysing the *Swift*/XRT data together with the *INTEGRAL* data (data set 1) we included a Gaussian component to model the Fe Kα emission line (Fig. 1), as the line is clearly detectable in the XRT spectrum. The Fe Kα line energy ($E \simeq 6.5 \pm 0.1$ keV) is consistent within the uncertainties with the value reported from *ASCA* data ($E = 6.48 \pm 0.08$ keV; Forster et al. 1999), from two *BeppoSAX* measurements ($E = 6.46 \pm 0.09$ and 6.38 ± 0.06 keV; Risaliti 2002), *Chandra* ($E = 6.36 \pm 0.02$ keV; Iwasawa et al. 2003) and *XMM–Newton* ($E = 6.39 \pm 0.01$ keV; Beckmann et al. 2004). The equivalent width (EW) of the iron line, as it can be derived from the *Swift*/XRT data, is comparably low with EW $= 202 \pm 20$ eV. This is close to the lower end of the observed range of EW $=$ 190–720 eV as found in the literature (Forster et al. 1999; Risaliti 2002; Iwasawa et al. 2003; Beckmann et al. 2004).

The best-fitting model to the overall spectra following the *F*-test statistics is model (ii) for both data sets (*F*-test probability of 97 per cent for data set 1 and 90 per cent for data set 2). This model gives an intrinsic absorption consistent with the one found in *ASCA* and *BeppoSAX* observations (Elvis et al. 2004), i.e. $N_H = 4 \times 10^{23}$ cm^{-2}, with a cut-off energy of $E_C = 209^{+44}_{-32}$ keV and a photon index $\Gamma = 1.70 \pm 0.04$ for the data set 2 and $N_H = 3 \times 10^{23}$ cm^{-2}, $E_C = 75^{+7}_{-6}$ keV and $\Gamma = 1.34 \pm 0.02$ for the data set 1. The reflection parameter is poorly constrained, and only an upper limit of $R < 0.5$ can be derived for both data sets (Table 3). The folded *INTEGRAL* spectra are shown in Fig. 2.

The parameters obtained for the summed *Swift*/XRT spectrum based on four short observations with quasi-simultaneous *INTEGRAL*/ISGRI data appear to differ from the spectral parameters of the whole *INTEGRAL* data set. These results, especially when compared to previous studies (Risaliti 2002; Beckmann et al. 2004; Fukazawa et al. 2007a,b; Shirai et al. 2008), point towards a significant X-ray spectral variability in NGC 4388. This motivated a study of the spectral shape with respect to the hard X-ray flux in the 20–60 keV band, as described in the next section.

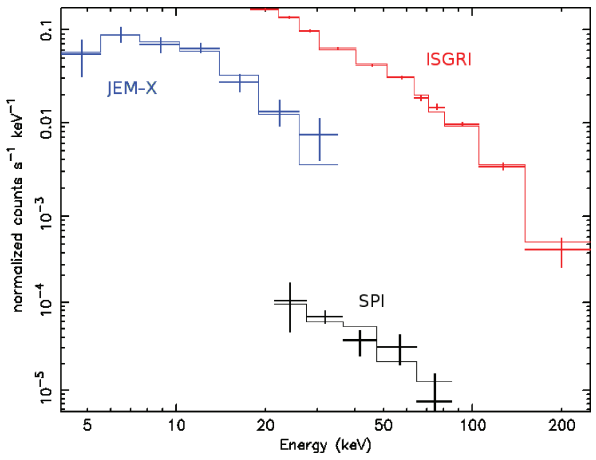

Figure 2. Folded *INTEGRAL* spectra based on the total exposure time.

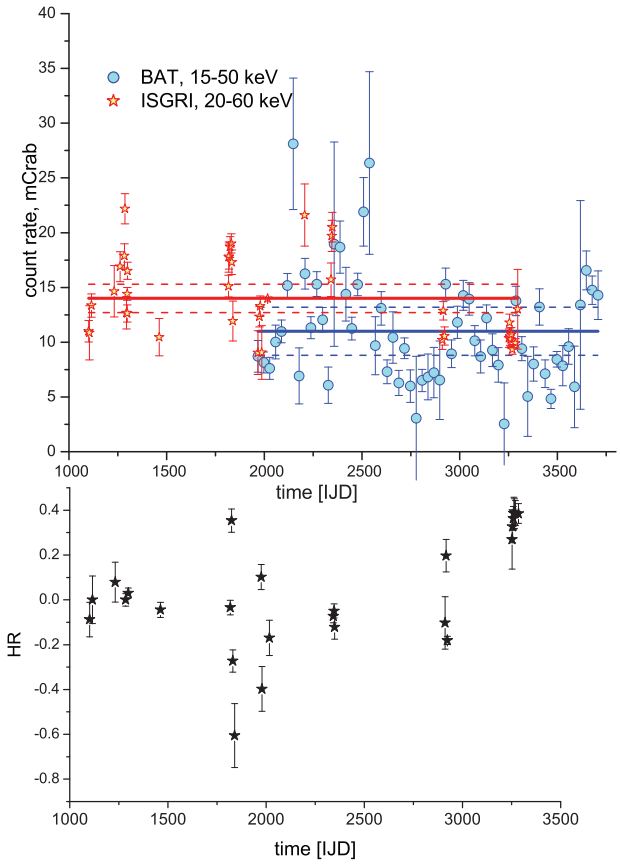

Figure 3. Top: *Swift*/BAT (15–50 keV) and *INTEGRAL* IBIS/ISGRI (20–60 keV) light curves. The mean values of the count rates and their 1σ errors are shown by the lines in the same colours as the corresponding light curve. Time is given in IJD (see footnote 3). Bottom: evolution of the hardness ratio with time.

4 VARIABILITY ANALYSIS

We extracted the light curve from *INTEGRAL* IBIS/ISGRI data in the 20–60 keV energy band to study the variability of NGC 4388 over the observational period. Time bins in this light curve are from 1 to 5 d, depending on the exposure times of observations in separate revolutions or close groups of revolutions. The ISGRI light curve together with the *Swift*/BAT light curve, with 30 d time bin, are shown in Fig. 3 (upper panel).[3] The mean value of the flux in the 20–60 keV energy band during the observational period is 14 mCrab.

We fitted separately the IBIS/ISGRI spectra corresponding to each revolution. In order to have a data set as uniform as possible we did not consider here the JEM-X data, which cover only a limited part of the ISGRI observations. To fit these data and to estimate the unabsorbed fluxes, the power-law model with exponential cut-off at high energies was applied with the hydrogen column density fixed to the value obtained for the total *INTEGRAL* spectrum (taking into

[3] Time is given in *INTEGRAL* Julian Date (IJD), which is defined as IJD = MJD – 51544.0. The origin of IJD is 2000 January 1 expressed in terrestrial time.

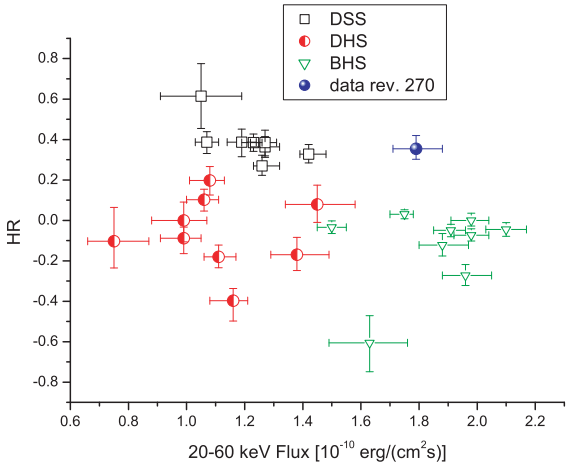

Figure 4. Hardness ratio versus 20–60 keV flux measured by IBIS/ISGRI.

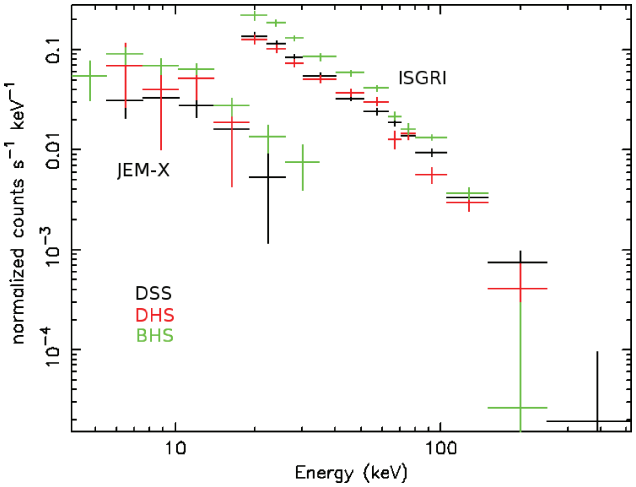

Figure 5. The spectra during the BHS, DSS and DHS phases (JEM-X and IBIS/ISGRI).

account that the reflection parameter obtained for the total spectrum best fit is compatible with 0, this model gave the same results as the *pexrav* one). We defined the hardness ratio as follows:

$$\mathrm{HR} = \frac{F_{60-500\,\mathrm{keV}} - F_{20-60\,\mathrm{keV}}}{F_{60-500\,\mathrm{keV}} + F_{20-60\,\mathrm{keV}}}. \quad (1)$$

Here $F_{20-60\,\mathrm{keV}}$ is the 20–60 keV flux and $F_{60-500\,\mathrm{keV}}$ is the flux above 60 keV (the upper energy boundary is varying from 200 to 500 keV from one observational period to another).

The dependencies of hardness ratio on time and on the 20–60 keV flux are reported in Figs 3 (lower panel) and 4, respectively. The correlation coefficient computed for the hardness ratio versus 20–60 keV flux relation is $R_{\mathrm{corr}} = 0.28$ with a corresponding probability of chance occurrence of $P_{\mathrm{corr}} = 0.1$, indicating that there is no significant correlation between these two quantities.

To see how the changes in the source flux correspond to changes in the spectrum, we split the data into three parts corresponding to three phases and compare the spectra. We define hereafter the 'bright, hard spectrum (BHS) phase' as characterized by the highest flux level (>14 mCrab) and a hardness ratio of HR < 0.2. In the 'dim, hard spectrum (DHS) phase' the source has <14 mCrab and has a similar hardness ratio as during the BHS phase. Finally, we define a 'dim, soft spectrum (DSS) phase' with low fluxes and a hardness ratio of HR > 0.2, i.e. softer than during the BHS and DHS phases. We use only those revolutions or pairs of revolutions which following each other directly (for instance, 89 and 90 together) and use only those revolutions with an exposure time ≥50 ks. The data revolutions corresponding to the BHS are 89–94, 207, 267, 268, 272–275 and 443–445; to the DHS are 28, 32, 320, 321, 334 and 633–637 and to the DSS are 747–759. For the other revolutions (30, 36, 71, 72, 78, 82, 148, 149, 324, 325, 397–399 and 762) the exposure times are not long enough to determine to which spectral phase they belong to. Only in revolution 270 the flux was on a high level and the hardness ratio was HR > 0.2, i.e. the source showed a bright and soft spectrum (BSS). For this phase only ISGRI data are available. We have modelled the spectra for these subsets separately. BHS, DHS and DSS spectra (both JEM-X and ISGRI) are shown together in Fig. 5.

To analyse the differences between the DSS, DHS and BHS spectra we fit the data obtained during these phases with model (ii) which is the best fit to the average *INTEGRAL* spectrum. We performed the modelling in two ways:

(i) 'fixed cut-off' case: the high-energy cut-off value is frozen to the best-fitting value of the average *INTEGRAL* spectrum, i.e. $E_{\mathrm{C}} = 209$ keV, and the other parameters (Γ, R and N_{H}) are left free to vary;

(ii) 'fixed reflection' case: R is put to 0 (the best-fitting value to the average *INTEGRAL* spectrum), while photon index, high-energy cut-off and hydrogen column density are free to vary.

When using the 'fixed cut-off' model ($\chi^2 = 13.2$ for the DSS phase, 13.8 during DHS phase and 15.2 for the BHS), the reflection parameter cannot be constrained for any of the different phases and only upper limits can be derived, consistent within the uncertainties for all phases and for the total average spectrum. For the same number of degrees of freedom, a smaller χ^2 is obtained when keeping the reflection parameter frozen and letting the cut-off energy free to vary (i.e. $\chi^2 = 10.6$ for the DSS phase, 13.1 during DHS phase and 13.9 for the BHS). The results of the spectral fitting with this model are shown in Table 4, together with the results for the ISGRI spectrum obtained during the particular revolution 270. Since no JEM-X data were available during this revolution, the hydrogen column density was fixed to $N_{\mathrm{H}} = 4 \times 10^{23}\,\mathrm{cm}^{-2}$, i.e. the value obtained for the average *INTEGRAL* spectrum.

Table 4. *INTEGRAL* best-fitting results for NGC 4388 during different phases. The errors are at the 90 per cent confidence level.

Phase, parameter	DSS	DHS	BHS	270[a]
χ^2/dof	10.6/13	13.1/12	13.9/13	4.6/7
Γ	1.87 ± 0.07	1.24 ± 0.12	1.51 ± 0.07	1.9 ± 0.2
E_{C} (keV)	>320	81^{+19}_{-14}	108^{+20}_{-15}	>185
N_{H} [b]	$6.4^{+2.4}_{-1.8}$	<7.9	$3.5^{+1.2}_{-1.0}$	4.0[c]
K_{X}	0.6 ± 0.1	1.1 ± 0.5	0.8 ± 0.1	–
$F_{4-20\,\mathrm{keV}}$ [d]	$0.83^{+0.02}_{-0.01}$	0.9 ± 0.1	$1.49^{+0.03}_{-0.04}$	–
$F_{20-60\,\mathrm{keV}}$ [d]	$1.21^{+0.03}_{-0.02}$	$1.14^{+0.06}_{-0.04}$	1.87 ± 0.05	$1.79^{+0.08}_{-0.09}$
$F_{60-200\,\mathrm{keV}}$ [d]	1.58 ± 0.04	$1.15^{+0.05}_{-0.04}$	1.76 ± 0.05	$2.3^{+0.2}_{-0.1}$
HR	$0.52^{+0.02}_{-0.03}$	$0.08^{+0.05}_{-0.03}$	$0.04^{+0.06}_{-0.05}$	$0.35^{+0.07}_{-0.06}$

[a] ISGRI spectrum obtained during data revolution 270.
[b] N_{H} given in units of $10^{23}\,\mathrm{cm}^{-2}$.
[c] Frozen value.
[d] Flux given in units of $10^{-10}\,\mathrm{erg\,cm}^{-2}\,\mathrm{s}^{-1}$.

With the 'fixed reflection' model, large variations of the cut-off energy as well as of the photon index are observed. Cut-off values of $E_C \simeq 110$ and $\simeq 80$ keV are measured during the BHS and DHS phases, respectively, and only a lower limit of $E_C > 320$ keV is found during the DSS phase. It was not possible to constrain the hydrogen column density of the DHS spectrum, and although the intrinsic absorption appears to be higher during the DSS phase than in the BHS one, the differences are significant only on a 2σ level. The photon indices during these phases show significant differences, with the DHS and BHS having harder spectra ($\Gamma = 1.24 \pm 0.12$ and 1.51 ± 0.07) than the DSS phase spectrum ($\Gamma = 1.87 \pm 0.07$).

5 DISCUSSION

We used broad-band (0.3–300 keV) *INTEGRAL* and *Swift* data collected over 6 yr in order to study the flux and spectral variability in the Seyfert 2 galaxy NGC 4388. Based on the *Swift*/BAT and *INTEGRAL*/ISGRI light curves (Fig. 3) we derive a maximum variability in flux by a factor of $\sim$2 in the 20–60 keV band on time-scales of 1–2 months. This is consistent with the flux variations by a factor of $\sim$1.8 as seen in the first 9 months of BAT observations (Beckmann et al. 2007a). Flux variations of this magnitude are common among type 2 AGN. Variability at hard X-rays can be higher than a factor of 10 on months time-scale, as seen e.g. in the BAT light curve of NGC 2992 (Beckmann, Gehrels & Tueller 2007b).

While our analysis covers time-scales larger than a month, studies based on *Suzaku* investigated the variability on time-scales shorter than a day (Fukazawa et al. 2007b). Their study revealed periodical variability of the primary continuum within hours. The variability observed with *Suzaku* was explained in terms of fluctuations of the accretion flow and/or disc instabilities.

Comparably slow variations of the 20–60 keV flux and of the spectral slope are shown here based on *INTEGRAL* data. The spectral shape changes do not seem to be directly linked to the flux level though. A more complex dependence on the physical conditions in the accreting/reflecting/absorbing media has to be assumed. Variations of these conditions lead to change of the spectral parameters and/or flux level in some energy band.

5.1 Absorption

Changes of the column density of an obscuring medium are among the common causes for soft X-ray variability in Seyfert 2 (Risaliti 2009). NGC 4388 is not an exception: absorption-induced variations were found in this object by Elvis et al. (2004).

The value of the column density in NGC 4388 obtained in our work is in the range $N_H = (2\text{–}7) \times 10^{23}$ cm^{-2}, confirming that this source is a Compton-thin type 2 AGN. This absorption strength is consistent with *XMM–Newton* measurements in 2002 ($N_H = (2.5\text{–}2.8) \times 10^{23}$ cm^{-2}; Beckmann et al. 2004), the results of two *Chandra* observations ($N_H = 2.5 \times 10^{23}$ cm^{-2}; Iwasawa et al. 2003, and $N_H = 3.5 \times 10^{23}$ cm^{-2}; Elvis et al. 2004) and two *ASCA* observations ($N_H = (2.2\text{–}4.3) \times 10^{23}$ cm^{-2}; Forster et al. 1999). Changes in the intrinsic absorption on the level mentioned above can explain the variability in the 2–10 keV band as shown by Elvis et al. (2004) studying *RXTE* data. However, the modest variability in absorption is not sufficient to explain the hard X-ray flux variations observed in the data presented here, and also seen by *Suzaku*, as at energies >20 keV Compton-thin absorbers have little influence on the observed flux. To confirm the last statement we have compared the values of unabsorbed fluxes in 20–60 keV band (for all phases as well as for the total exposure spectra) with those obtained for different frozen values of column density within $N_H = (1\text{–}8) \times 10^{23}$ cm^{-2}. Only negligible differences were found.

5.2 Spectral slope and high-energy cut-off

Throughout the years we observe spectral variability in NGC 4388. The best-fitting model to the total exposure time spectrum is an absorbed power law with an upper limit on the Compton reflection component ($R < 0.5$), a high-energy cut-off near 210 keV and a spectral slope of $\Gamma = 1.7$. The value of the photon index is close to the mean value of $\langle\Gamma\rangle = 1.8$ derived from *BeppoSAX* observations of Seyfert 2 galaxies (Dadina 2007), but the cut-off energy in NGC 4388 appears to be significantly lower than the average value of $\langle E_C\rangle = 376 \pm 42$ keV.

However, as we can see from the results of our spectral modelling obtained during the different phases, the shape of the 20–300 keV spectrum of NGC 4388 varies both in photon index and cut-off energy. The lowest value of cut-off energy, obtained during the DHS phase, is $E_C \simeq 80$ keV. This and the value of the spectral slope $\Gamma = 1.24$ measured during this phase are consistent within the errors with the values obtained by Beckmann et al. (2009) based on the first 870 ks of *INTEGRAL*/ISGRI observations (i.e. $E_C = 80$ keV and $\Gamma = 1.3$). The high-energy cut-off of NGC 4388 measured in *Suzaku* data (Shirai et al. 2008) appears to be even lower, with a value of $E_C = 30$ keV and an even harder spectral slope of $\Gamma = 0.9$.

We find both 'hard spectrum' and 'soft spectrum' phases with a high level of 20–60 keV flux as well as with a low one. Thus the spectral shape does not appear to be directly linked to the flux level, especially taking into account the previous work by Beckmann et al. (2004).

In NGC 4388 we observe at least four different types of variations:

(i) 2–10 keV variability due to changes of the density of an obscuring medium (Elvis et al. 2004);

(ii) fast intraday variations of the intrinsic nuclear emission at 3–200 keV, likely due to fluctuations in the accreting flow and/or disc instabilities (Fukazawa et al. 2007b);

(iii) broad-band flux changes with stable spectral shape (Beckmann et al. 2004) which can be caused by variations of the amount of accreting plasma (total or visible to the observer) in the hot corona surrounding the central black hole (Beckmann et al. 2007b);

(iv) variations of the spectral shape in the 20–300 keV energy range (this work).

The latter can be caused by instabilities in the accretion flow (i.e. temperature and density of the plasma in the corona, inner radius of the accretion disc, etc.) in a way described e.g. by Czerny (2003).

5.3 NGC 4388 and other objects: differences and similarities

The behaviour we observe in NGC 4388 appears to be reversed to what was reported in the case of the brightest AGN at hard X-rays, the Seyfert 1.5 galaxy NGC 4151 (Lubiński et al. 2010). The data on this source revealed a high state with a plasma temperature of $T = 50\text{–}70$ keV with high optical depth ($\tau = 1.3\text{–}2.6$) and a low state with $T = 180\text{–}230$ keV and $\tau = 0.3\text{–}0.7$. Lubiński et al. interpreted the results as observations of an inner hot accretion surrounded by an outer cold disc.

An example of variations like the one we observe in NGC 4388 can be found in the Seyfert 1 galaxy IC 4329A (Soldi et al. 2010). In this object a high-energy cut-off near 40 keV was found in the 2003 August *INTEGRAL*/ISGRI observations but no cut-off was detected

in 2003 July. At the same time, the flux did not show significant variability.

Other objects with hard X-ray to γ-ray spectral shape variable on months time-scales are e.g. the Seyfert 1 galaxies NGC 5548 (Nicastro et al. 2000) and NGC 3783 (De Rosa et al. 2002), the narrow line Seyfert 1 galaxy NGC 5506 (Manchanda 2006) and the Seyfert 2 galaxy NGC 2110 (Beckmann & Do Cao 2011). The first three of these objects follow the pattern predicted by the two-phased, non-pair-dominated AGN/X-ray background (XRB) model by Poutanen & Svensson (1996). They show a behaviour similar in some sense to Galactic black holes (GBHs): steepening of the primary continuum when the source brightens, i.e. the flux level is correlated with the spectral slope. A cut-off at high energies was seen only in NGC 5548, and here only in the dim state.

In any case, the non-pair-dominated AGN/XRB model cannot be applied to NGC 4388 because this source does not show a correlation of flux level and spectral slope. In fact, the DSS and DHS phases have very similar fluxes with significantly different spectral parameters. To explain the variations observed in this AGN we suggest a more complex scenario, for instance that both density and temperature of the plasma in the corona change and also the disc/corona geometry is variable, similar to the scenarios presented by Uttley et al. (2003) and Petrucci et al. (2004).

The behaviour of NGC 2110 and of NGC 5506 (in recent observations; Soldi et al. 2011) appears to be more similar to NGC 4388, i.e. spectral slopes and fluxes seem to vary independently. Still, those two objects differ from NGC 4388, because both cut-off at low energies. NGC 5506 has cut-off values in the range 40–100 keV and a softer ($\Gamma = 1.9$) average spectrum than NGC 4388, while the cut-off in NGC 2110 appears to be persistent at $E_{\rm C} \simeq 80$ keV, whereas for NGC 4388 it varies with time, not being directly correlated with the flux level.

For AGN, as well as for GBH systems, the low flux state with a hard spectrum and high-energy cut-off is supposed to be connected to radio-loud objects which display a jet (Ho 2005) or other types of outflows. The narrow line Seyfert 1 galaxy NGC 5506 is indeed a radio-quiet AGN (Gallimore et al. 2006) with a cut-off in the range 40–100 keV, while NGC 2110 is radio loud with a cut-off near 80 keV (Beckmann & Do Cao 2011). NGC 4388 is a radio-quiet object despite the presence of a radio outflow (Gallimore et al. 2006). This brings up the question about the radio emission of this AGN – is it permanently weak or are there periods of comparatively high radio luminosity? Is the radio luminosity of this object connected to the flux and the spectral parameters in the X-ray band?

6 CONCLUSIONS

We have performed an analysis of the *INTEGRAL* data obtained for NGC 4388 during the period 2003 January to 2009 July, together with quasi-simultaneous data from *Swift*. The main results found from the data obtained the 6 yr of *INTEGRAL* observations of NGC 4388 can be summarized as follows:

(i) the flux variability on time-scales of 3–6 months in the 20–60 keV energy range is of the order of a factor of $\sim$2;

(ii) significant spectral shape changes of the 20–300 keV spectrum are observed, uncorrelated with the flux level;

(iii) the lower value of the exponential cut-off at high energies (found during the hard spectrum phase) is similar to that of radio-loud AGN. However, NGC 4388 is a radio-quiet object.

This flux and spectral shape variability is not induced by changes of the intrinsic absorption. The spectral variability detected here is rather peculiar for Seyfert 2 type objects. However, it is possible that in the near future we will discover more AGN with similar properties, especially taking into account the fast growth of both the amount and the quality of high-energy data on extragalactic objects.

The possible causes of the variability described above lie in the unstable conditions within the central engine, from changes of the temperature in the hot corona to perturbations in the inner part of the accretion disc due to ejections.

In GBH systems the hard/soft variations are supposed to be connected with radio ejections/jet activity. Thus it would be interesting to test this link in AGN, e.g. to observe NGC 4388 simultaneously in hard X-rays/γ-rays and at radio frequencies to trace out the link between the radio luminosity and spectral shape in X-rays/γ-rays.

ACKNOWLEDGMENTS

This research has made use of data obtained through the High Energy Astrophysics Science Archive Research Center. Online Service, provided by the NASA/Goddard Space Flight Center, and is based on observations with INTEGRAL, an ESA project with instruments and science data centre funded by ESA member states (especially the PI countries: Denmark, France, Germany, Italy, Switzerland, Spain), Poland and with the participation of Russia and the USA. We acknowledge the use of *Swift*/BAT transient monitor results provided by the *Swift*/BAT team. EVF is thankful to the Virtual Roentgen and Gamma Observatory (VIRGO.UA) centre in Kiev for offering informational and technical facilities. EVF is also grateful to V. Bianchin and L. Foschini for their help with the *INTEGRAL* software.

REFERENCES

Antonucci R., 1993, ARA&A, 31, 473
Arnaud K. A., 1996, in Jacoby G., Barnes J., eds, ASP Conf. Ser. Vol. 101, Astronomical Data Analysis Software and Systems V. Astron. Soc. Pac., San Francisco, p. 17
Barthelmy S. D. et al., 2005, Space Sci. Rev., 120, 143
Beckmann V., Do Cao O., 2011, in Proc. 8th INTEGRAL Workshop, preprint (arXiv:1102.4974)
Beckmann V., Gehrels N., Favre P., Walter R., Courvoisier T. J.-L., Petrucci P.-O., Malzac J., 2004, ApJ, 614, 641
Beckmann V., Barthelmy S. D., Courvoisier T. J.-L., Gehrels N., Soldi S., Tueller J., Wendt G., 2007a, A&A, 475, 827
Beckmann V., Gehrels N., Tueller J., 2007b, ApJ, 666, 122
Beckmann V. et al., 2009, A&A, 505, 417
Bian W., Gu Q., 2007, ApJ, 657, 159
Caroli E., Stephen J. B., Di Cocco G., Natalucci L., Spizzichino A., 1987, Space Sci. Rev., 45, 349
Courvoisier T. J.-L. et al., 2003a, A&A, 411, L53
Courvoisier T. J.-L. et al., 2003b, A&A, 411, L343
Czerny B., 2003, in Collin S., Combes F., Shlosman I., eds, ASP Conf. Ser. Vol. 290, Active Galactic Nuclei: From Central Engine to Host Galaxy. Astron. Soc. Pac., San Francisco, p. 59
Dadina M., 2007, A&A, 461, 1209
De Rosa A., Piro L., Fiore F., Grandi P., Maraschi L., Matt G., Nicastro F., Petrucci P. O., 2002, A&A, 387, 838
Dewangan G. C., 2001, Bull. Astron. Soc. India, 29, 463
Elvis M., Risaliti G., Nicastro F., Miller J. M., Fiore F., Puccetti S., 2004, ApJ, 615, L25
Forster K., Leighly K. M., Kay L. E., 1999, ApJ, 523, 521
Fukazawa Y. et al., 2007a, Progress Theor. Phys. Suppl., 169, 282
Fukazawa Y. et al., 2007b, in Ho L. C., Wang J.-M., eds, ASP Conf. Ser. Vol. 373, The Central Engine of Active Galactic Nuclei. Astron. Soc. Pac., San Francisco, p. 165

Gallimore J. F., Axon D. J., o'Dea C. P., Baum S. A., Pedlar A., 2006, AJ, 132, 546
Gehrels N. et al., 2004, ApJ, 611, 1005
Hanson C. G., Skinner G. K., Eyles C. J., Willmore A. P., 1990, MNRAS, 242, 262
Ho L. C., 2005, Ap&SS, 300, 219
Iwasawa K., Fabian A. C., Ueno S., Awaki H., Fukazawa Y., Matsushita K., Makishima K., 1997, MNRAS, 285, 683
Iwasawa K., Wilson A. S., Fabian A. C., Young A. J., 2003, MNRAS, 345, 369
Lebrun F. et al., 2003, A&A, 411, L141
Lubiński P., Zdziarski A., Walter R., Paltani S., Beckmann V., Soldi S., Ferrigno C., Courvoisier T. J.-L., 2010, MNRAS, 408, 1851
Lund N. et al., 2003, A&A, 411, L231
Magdziarz P., Zdziarski A. A., 1995, MNRAS, 273, 837
Manchanda R. K., 2006, Advances Space Res., 38, 1387
Mas-Hesse J. M. et al., 2003, A&A, 411, L261
Nicastro F. et al., 2000, ApJ, 536, 718
Petrucci P. O., Maraschi L., Haardt F., Nandra K., 2004, A&A, 413, 477
Phillips M. M., Malin D. F., 1982, MNRAS, 199, 905
Poutanen J., Svensson R., 1996, ApJ, 470, 249
Risaliti G., 2002, A&A, 386, 379
Risaliti G., 2009, in Peterson B. M., Sommerville R. S., Storchi-Bergmann T., eds, Proc. IAU Symp. 267, Co-evolution of Central Black Holes and Galaxies. Cambridge Univ. Press, Cambridge, p. 119
Shirai H. et al., 2008, PASJ, 60, 263
Soldi S., Ponti G., Beckmann V., Lubiński P., 2010, in Proc. The Extreme Sky: Sampling the Universe Above 10 keV, preprint (arXiv:1001.4348)
Soldi S., Beckmann V., Gehrels N., De Jong S., Lubiński P., 2011, in Proc. Workshop Narrow-Line Seyfert 1 Galaxies and Their Place in the Universe, preprint (arXiv:1105.5993)
Tueller J., Mushotzky R. F., Barthelmy S., Cannizzo J. K., Gehrels N., Markwardt C. B., Skinner G. K., Winter L. M., 2008, ApJ, 681, 113
Uttley P., Edelson R., McHardy I. M., Peterson B. M., Markowitz A., 2003, ApJ, 584, L53
Vedrenne G. et al., 2003, A&A, 411, L63
Winkler C. et al., 2003, A&A, 411, L1

This paper has been typeset from a TEX/LATEX file prepared by the author.